Geochemistry Geophysics Geosystems G3

Article
Volume 00, Number 00
0 MONTH 2013
doi: 10.1002/ggge.20171
ISSN: 1525-2027

Published by AGU and the Geochemical Society

Subduction and slab breakoff controls on Asian indentation tectonics and Himalayan western syntaxis formation

Fabio A. Capitanio
School of Geosciences, Monash University, Clayton, Victoria 3800 Australia (fabio.capitanio@monash.edu)

Anne Replumaz
Institute des Sciences de la Terre, Université de Grenoble 1, CNRS, Grenoble, France

[1] We test the link between large-scale Asian continent deformations and Indian slab subduction and breakoff during convergence by means of three-dimensional numerical models of the subducting-upper plates system. We find that the subduction of the buoyant continent results in the reduction of convergence velocity comparable to that observed in the Indian motions, yet the upper plate deformation remains accommodated in a narrow belt along a straight margin. Comparable rates are measured when the subducting slab breakoff is modeled, although the convergent margin deforms and curves markedly, with large underplating contiguous to ongoing subduction, similar to what observed along the Himalayan range. The models support the interpretation of the Himalayan Western Syntaxis evolution, the progressive curvature of the Indian margin and the underthrusting as a consequence of the Indian slab breakoff. The modeled slab detachment is followed by short-lived large stresses in the upper plate interiors, propagating at large distance from the margin with a trend similar to several major Asian lithospheric faults. Such localized stress has likely provided the conditions for the formation of the Central Asian intracontinental faulting, the Bangong-Red River and the Altyn Tagh faults, that followed successive Indian slab breakoff episodes. Continent subduction and breakoff during India-Asia convergence offer an explanation for the different deformation mechanisms as the long-lived understhrusting and the episodic lithospheric faulting in the Asian continent and their link to deep processes.

Components: 10,478 words, 10 figures.

Keywords: subduction; slab breakoff; continental tectonics; asian tectonics; Himalayan western syntaxis.

Index Terms: 3040 Plate tectonics: Marine Geology and Geophysics; 8104 Continental margins: convergent: Tectonophysics; 8150 Plate boundary: general: Tectonophysics; 8155 Plate motions: general: Tectonophysics; 8157 Plate motions: past: Tectonophysics; 8158 Plate motions: present and recent: Tectonophysics; 8170 Subduction zone processes: Tectonophysics.

Received 26 February 2013; **Revised** 2 May 2013; **Accepted** 8 May 2013; **Published** 00 Month 2013.

Capitanio, F. A., and A. Replumaz (2013), Subduction and slab breakoff controls on Asian indentation tectonics and Himalayan western syntaxis formation, *Geochem. Geophys. Geosyst.*, *14*, doi:10.1002/ggge.20171.

© 2013. American Geophysical Union. All Rights Reserved.

1. Introduction

[2] The indentation of the Indian plate into the Asian lithosphere is one of the most spectacular features of plate tectonics; however, how the Asian tectonics is coupled to the deep process of Indian subduction remains unknown. The northward migration of the rigid Indian plate acted like an indenter, deforming the whole Asian continent interiors [*Molnar and Tapponnier*, 1975]. Different deformation mechanisms accommodate the convergence in Central Asia, at the front of the indenting Indian plate. Major lithospheric faulting deformed episodically the Asian continent, at large distance from the convergent margin, as the Bangong-Red River fault (RRF), and later the Altyn Tagh fault (ATF) [*Meyer et al*., 1998; *Tapponnier et al*., 2001]. In the east, the Tibetan plateau has progressively thickened during the northward migration of the Indian plate [*England and McKenzie*, 1982; *England and Houseman*, 1985]; instead, more to the west the convergence was accommodated by large underthrusting, forming the Western Syntaxis [*Burtman and Molnar*, 1993].

[3] Several works have investigated the coupling between Asian deformation and the large-scale convergence. Analogue models have explored the influence of convergence and breakoff on underthrusting of the Indian lithosphere [*Chemenda et al*., 2000]. Other modeling effort considered the force balance between the imposed Indian convergence and the thickening of the Tibetan plateau [*Royden et al*., 2008; *England and Houseman*, 1985; *Tapponnier et al*., 2001], and the controls these boundary conditions have on Central Asian lithospheric faulting [*Molnar and Tapponnier*, 1975; *Tapponnier and Molnar*, 1976]. In fact, these three different deformation mechanisms are not easily reconciled and their occurrence along the India-Asia convergent margins is, to date, unexplained.

[4] The Indian subducting margin evolved from a rather linear feature during the closure of the Tethys to a progressively curved margin following the Greater Indian continent subduction [*Hafkenscheid et al*., 2006; *Replumaz et al*., 2004; *Van der Voo et al*., 1999]. During this later stage, the Greater Indian slab detached repeatedly [*Replumaz et al*., 2004; *Replumaz et al*., 2010a]. Although it has been suggested that the Central Asian complex tectonics must be rooted in the subduction dynamics [*Mattauer et al*., 1999], the relation between the complex subduction history and the Central Asian tectonics is yet unexplored.

[5] Here we investigate on the link between deep processes and continental tectonics at convergent margins addressing the role the continent subduction and slab breakoff play on the development of continental tectonics during convergence. We present a suite of three-dimensional numerical models that reproduce the self-consistent force balance between the subducting and the overriding lithospheres and the mantle and we discuss the insights these offer into the Asian tectonics.

1.1. Indian Mantle Tomography

[6] Beneath the present-day position of India, remnants of the Tethys slab are found at depth greater than 1000 km [*Hafkenscheid et al*., 2006; *Van der Voo et al*., 1999], whereas the subducted Indian lithosphere lay at shallower depth [*Replumaz et al*., 2010b] (Figure 1). The Indian slab appears disconnected laterally from the South-East Asian and Arabian slabs, and from the Tethys slab beneath [*Replumaz et al*., 2010b]. This indicates that the Tethyan slab ruptured and the Indian lithosphere separated from the neighboring slabs, while advancing northward, although possibly was separated earlier [*Zahirovic et al*., 2012]. At depth larger than ~1000 km, the Tethys slab has a rather linear shape [*Negredo et al*., 2007], suggesting that the subducting margin was near linear during the Mesozoic closure of the Tethys.

[7] The subhorizontal tear interrupting the vertical continuity of the slab at ~1000 km depth in the tomography has been interpreted as a complete breakoff occurring at the Ocean-Continent Boundary (OCB), that completely detached the Tethys from the Indian continental slab at ~45 Ma (anomaly TH, Figure 1, *Negredo et al*. [2007]).

[8] After the Tethys slab breakoff event, Indian lithosphere subduction resumed in the central part of the continent, between 40 and 30 Ma. In this time, the convergent margin increasingly curved during the northward migration of India, reaching large northward offset respect to the present-day location of the lower mantle Tethys anomaly [*Replumaz et al*., 2010b] (Figures1c and 1d, anomaly IN). The western end of the Indian lithosphere is now found at shallow depth, underplating largely the Asian lithosphere, and subducting northward beneath the Hindu Kush (Figure 1a, anomaly HK) [*Li et al*., 2008; *Negredo et al*., 2007]. At depth, a vertical tear has been inferred

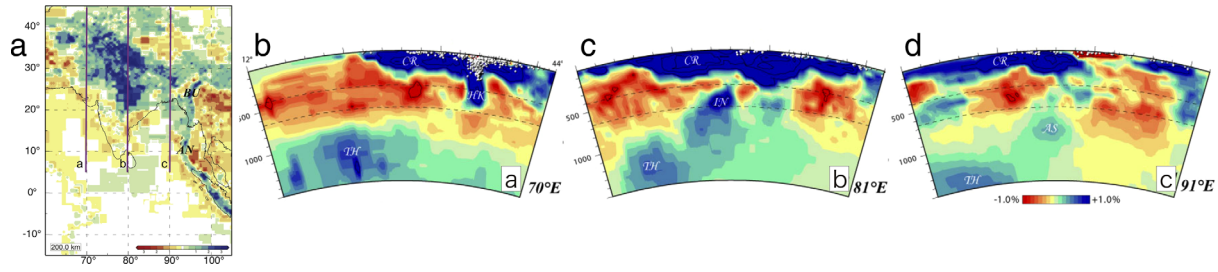

Figure 1. Tomographic model of the India-Asia area. (a) Tomographic section at 200 km depth, showing wave speed anomaly at ±3%. Strong positive anomalies (+2–3%, blue) mark the cold Indian oceanic plate subducting beneath Indonesia and the cold lithospheric mantle beneath the Indian craton. Weaker positive anomalies (+1–2%) mark the other Asian cratons, and the thickening of the Tien Shan. (b–d) Vertical cross sections through the India-Asia convergent margin. See Figure 1a for location. The contour interval is 1%. Modified after *Replumaz et al*. [2012], and *Negredo et al*. [2007].

to between the western (HK) and central (IN) portions of the Indian slab [*Replumaz et al*., 2010b].

[9] In the late stage of the convergence, a second episode of Indian slab breakoff has been reconstructed. A subhorizontal tear occurred within the central continental slab (IN) and propagated from its westernmost border toward the east, over a time span of ∼10 myr between 25 and 15 Ma [*Replumaz et al*., 2010b].

[10] In the present day, the western Indian lithosphere extends as far as ∼300 km from the Main Frontal Thrust (MFT), reaching the Hindu Kush [*Burtman and Molnar*, 1993; *Mechie et al*., 2012], where it subducts reaching depths of ∼600 km [*Koulakov and Sobolev*, 2006; *Negredo et al*., 2007] (Figure 1b). In the east, the Indian plate extends progressively north of the Tsangpo suture (Figure 1c), and beneath Central Tibet extends ∼400 km north of the MFT, reaching to the Bangong suture [*Kind and Yuan*, 2010; *Kosarev et al*., 1999; *Kumar et al*., 2006; *Nábelek et al*., 2009; *Yuan et al*., 1997], where locally sinks in the mantle reaching large depth [*Li et al*., 2008]. The westernmost Indian lithosphere as imaged in global tomography has retained the curved shaped achieved during convergence (Figure 1a).

1.2. India-Asia Convergence and Central Asia Tectonics

[11] India-Asia convergence rates in excess of 15–18 cm yr^{-1} were recorded during the Mesozoic, until ∼50 Ma [*Patriat and Achache*, 1984], while deformation on the upper plate was located mostly along a narrow belt at the Asian margin [*Murphy et al*., 1997]. Between ∼50 and 40 Ma, the convergence rate progressively dropped, reaching values between 4 and 7 cm yr^{-1} from 40 Ma onward [*Molnar and Stock*, 2009; *Patriat and Achache*, 1984]. This relative convergence rate decrease associated with the 50–40 Ma transient coincides with the initiation of the widespread Asian continental tectonics [*Molnar and Tapponnier*, 1975; *Tapponnier and Molnar*, 1976] and the entrainment of part of the Greater Indian continent into subduction [*Mattauer*, 1986]. In this time, deformation in the upper plate migrated from the Asian margin to the continent interiors (Figure 2a) and likely follows the reconstructed breakoff episode, ∼45 Ma. In this early stage, the deformation migrated eastward along the Bangong suture, which initiated close to the western corner of the Indian continent. It later connected to the RRF and led to the eastward extrusion of the Indochina block [*Briais et al*., 1993; *Leloup et al*., 2001], which is correlated to the retreat of the southeastern Asian margin [*Replumaz et al*., 2004] (Figure 2b). The Karakorum fault activated by ∼25 Ma [*Leloup et al*., 2011] further separating the westernmost Himalayan front from the Tarim basin. The Tibetan plateau is bounded to the north by the Asian southward subduction zone in the Pamir, and to the west by the Chaman fault, forming the Himalayan Western Syntaxis. Farther north, the structures of the Tien Shan activated by ∼23 Ma [*Yin*, 2010], trending northeastward from the Hindu Kush front, on the westernmost edge of the Indian margin, deforming the Asian continent interiors. Between 20 and 17 Ma the convergence velocity drops, reaching abruptly less than 5 cm yr^{-1} [*Molnar and Stock*, 2009] and has remained to similar values since. As the extrusion of the Indochina block out of the convergence direction was completed, the central Asian tectonics migrated north, taking active deformation more than 1000 km in the Asian continent interior along the ATF [*Meyer et al*., 1998; *Replumaz and*

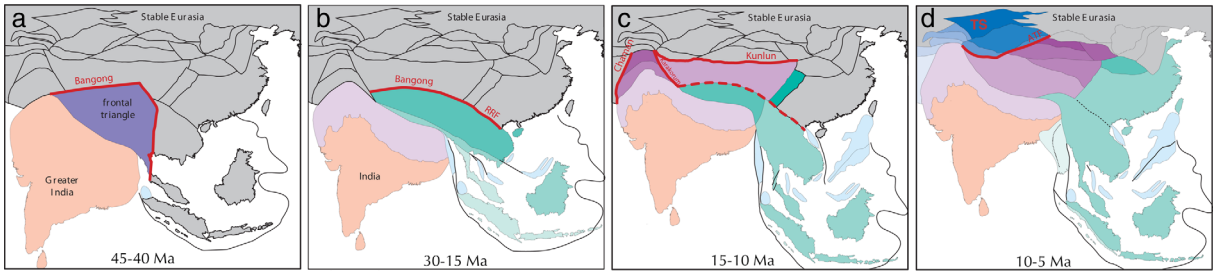

Figure 2. Reconstruction of the block kinematics and tectonics of the India-Asia convergence area. Reconstructed positions at (a) 45–40 Ma, (b) 30–15 Ma, RRF is for Red River Fault, and (c) 15–0 Ma, TS is for Tien Shan, BS for Bangong Suture. Color coding is for the areas of active tectonics during the time interval, gray for tectonically quiescent areas. Modified after *Replumaz and Tapponnier* [2003].

Tapponnier, 2003; *Tapponnier et al*., 2001] (Figure 2c). This fault initiated with a similar strike and right-lateral kinematics to the Bangong-RRF [*Tapponnier et al*., 2001].

2. Numerical Modeling

2.1. Modeling Approach

[12] In this work we focus on the interactions between downgoing and overriding plates in a subduction system. Continent subduction is modeled through the different integrated buoyancies of continental and oceanic subducting lithospheres, following *Capitanio et al*., 2010a, and *Capitanio et al*., 2011. This allows modeling the slab mass variation in time and space along the convergent margin that follow continent subduction and slab breakoff and provides the understanding of their impact on the force balance driving plate convergence and deformations.

[13] Here we address also the role of slab breakoff during subduction. Slab breakoff, or slab detachment, is the separation of the deep portion of a lithospheric slab from the subducting plate. Tomographic evidence of this process suggests breakoff typically occurs when the OCB subducts at shallow depths [*Chemenda et al*., 2000; *Regard et al*., 2005; *Wortel and Spakman*, 2000] although this has been observed also to occur within oceanic plates [*Levin et al*., 2005]. Causes for the plate rupture during subduction are the excess stress the lithosphere undergoes at the hinge bending at subduction zone [*Wong A Ton and Wortel*, 1997], the tensile stresses at the OCB when this is subject to the pull of an oceanic slab [*Davies and von Blanckenburg*, 1995], or also due to additional forcing provided by the overpressuring of the sub-slab mantle [*Liu and Stegman*, 2011, 2012]. Lateral propagation of slab detachment likely occurs by stress focusing on the rupture tip, triggering further rupture [*Yoshioka and Wortel*, 1995], which can reach very high rates [*Burkett and Billen*, 2010; *van Hunen and Allen*, 2011], and large mass of slab can be lost abruptly. Many studies exist on the rupture mechanics and the implication for the geophysical observable around subduction zones [e.g., *Buiter et al*., 2002; *Duretz et al*., 2012; *Gerya*, 2011; *Gerya et al*., 2004, and references therein]. Here we focus on the implications of slab loss and thus we do not address the details of rupture mechanics. Instead, this is modeled here by varying the yield strength of the subducted oceanic plate. Then, the spontaneous localization of large stresses at the OCB leads to localized rupture as in the published models.

[14] The parameters of the breakoff investigated are the width of the slab detachment w, and the propagation speed. The width of the slab detachment is either limited to a portion of the slab, 500 and 1000 km wide, where yield strength is locally lowered, or to a width that is equal to the slab width, that is the slab is completely removed during subduction. For the yield strength chosen, the breakoff occurs at a depth of ~100 km, the intermediate depth of *Duretz et al*., [2012], that is when the tensile stresses are maximized. We have also tested the two propagation modalities according the recent modeling of *Burkett and Billen* [2010], and *van Hunen and Allen* [2011]: a breakoff occurring simultaneously along the wide slab and one propagating at a finite rate. This is done in the models by reducing the slab limit stress, i.e., the cohesion, to a very low strength (Table 1), resulting in the simultaneous yielding along the margin, and to a relatively higher value of the cohesion, resulting in the slower propagation of the tear by stress localization [e.g., *Yoshioka and Wortel*, 1995], once the tear has been triggered on the edge through a lower yield stress.

Table 1. Model Parameters Used in the Experiments

Quantity	Symbol	Value
Gravitational acceleration	g	9.81 m s^{-2}
Reference viscosity	η_0	2×10^{20} Pa s
Reference density	ρ_0	3300 kg m^{-3}
Reference cohesion	C_0	48 MPa
Friction coefficient	μ	0.42
Upper mantle thickness		660 km
Upper mantle viscosity	η_{UM}/η_0	2×10^{20} Pa s
Lower mantle viscosity	η_{LM}	$10^2\eta_0$
Subducting plate initial length		2500 km
Subducting plate width		2500 km
Subd. plate viscosity (0–70 km)		$3\times10^3\eta_0$
Subd. plate viscosity (70–100 km)		$3\times10\eta_0$
Plastic crust thickness		30 km
Continental plate initial length		1700 km
Oceanic plate initial length		800 km
Continental plate density contrast	$\Delta\rho_C$	80, 53.3, 26.6 kg m^{-3}
Oceanic plate density contrast	$\Delta\rho_0$	80 kg m^{-3}
Oceanic plate cohesion		$2\times C_0$, C_0
Breakoff width	w	
Upper plate thickness		50 km
Upper plate density contrast		0 kg m^{-3}
Upper plate viscosity	η_{UP}	

2.2. Methodology and Setup

[15] Subduction is modeled as the incompressible, viscous flow of an infinite Prandtl number fluid at very low Reynolds number. Under these approximations, the force balance is governed by the conservation of mass, enforcing the incompressibility condition, and momentum equations:

$$\nabla \cdot \mathbf{u} = 0 \tag{1}$$

$$\nabla \cdot \sigma = \mathbf{f} \tag{2}$$

where $\mathbf{u}$ is the velocity vector, σ the stress tensor and $\mathbf{f} = \rho\mathbf{g}$ the force term, with ρ the density and $\mathbf{g}$ the gravity vector. The stress tensor splits into a deviatoric part, τ, and an isotropic pressure p:

$$\sigma = \tau - p\mathrm{I} \tag{3}$$

where I is the identity tensor. The constitutive equation relating the stresses with the velocity gradients is given by the generalized Newtonian model of the form:

$$\tau = \frac{1}{2}\eta\left(\nabla\mathbf{u} + (\nabla\mathbf{u})^{\mathrm{T}}\right) = 2\eta\dot{\varepsilon}, \tag{4}$$

where η is the dynamic viscosity and $\dot{\varepsilon}$ is the strain rate tensor. Plasticity is implemented using a Byerlee's law for the definition of the yield stress as:

$$\tau_Y = C_0 + \mu p \tag{5}$$

where C_0 is the cohesion at zero confining pressure and μ is the friction coefficient. The composite visco-plastic flow law used in the models is implemented through the effective viscosity:

$$\eta_{eff} = \min\left(\eta, \frac{\tau_Y}{2\dot{\varepsilon}_{II}}\right) \tag{6}$$

where $\dot{\varepsilon}_{II} = \sqrt{\dot{\varepsilon}_{ij}\,\dot{\varepsilon}_{ij}/2}$ is the second invariant of the strain rate tensor. Similarly, we define the second invariant of the stress tensor as $\tau_{II} = \sqrt{\tau_{ij}\,\tau_{ij}/2}$.

[16] We solve equations (1) and (2) in their nondimensionalized form using a Particle-in-cell finite element method, Underworld [*Moresi et al.*, 2003], where Lagrangian integration points are embedded in a three-dimensional Eulerian mesh of $96 \times 96 \times 64$ elements. The details of the numerical method, software implementation and relevant numerical benchmarks are described in [*Moresi et al.*, 2003; *Stegman et al.*, 2006].

[17] The model space is a 3-D Cartesian box, 4000 km long, 4000 km wide, and 1000 km deep. Periodic boundary conditions are enforced on the front and rear walls ($x = 0$, 4000 km), free-slip on top and sidewalls, no-slip on the bottom and a symmetry plane in $y = 0$ (Figure 3). We do not account for Earth's sphericity since it has a negligible role on the subduction dynamics, also for the trench width tested here [*Morra et al.*, 2006].

[18] The ambient mantle is a Newtonian fluid of viscosity of $\eta_M = 2 \times 10^{20}$ Pa s, used here as reference viscosity η_0 (Figure 3b and Table 1). The lower mantle, below 660 km depth, has a viscosity of $10^2\eta_0$ and density increase of +80 kg m^{-3}. The subducting lithosphere is 2500 km wide layered in a 70 km thick top layer, of viscosity of $10^3\eta_0$, and a 30 km thick bottom layer of viscosity of $10\eta_0$. The topmost 30 km of the lithosphere use a composite visco-plastic rheology. The subducting plate-mantle density contrast chosen is $\Delta\rho_O = 80$ kg m^{-3}, for the oceanic domain (O in Figure 3a), and for the domain C we use $\Delta\rho_C = 80$, that is no buoyancy variation in the subducting plate, and 53.3 and 26.6 kg m^{-3} (C in Figure 3a). The resulting integrated buoyancy values of these latter are compatible with that of continental lithospheres with an eclogitic/amphibolitic crust [*Cloos*, 1993]. The buoyancy of the oceanic plate is sufficient to drive subduction from an initial condition of an incipient slab, extending to 150 km depth.

[19] The model's upper plate has no density contrast with the mantle, an initial thickness of 40 km

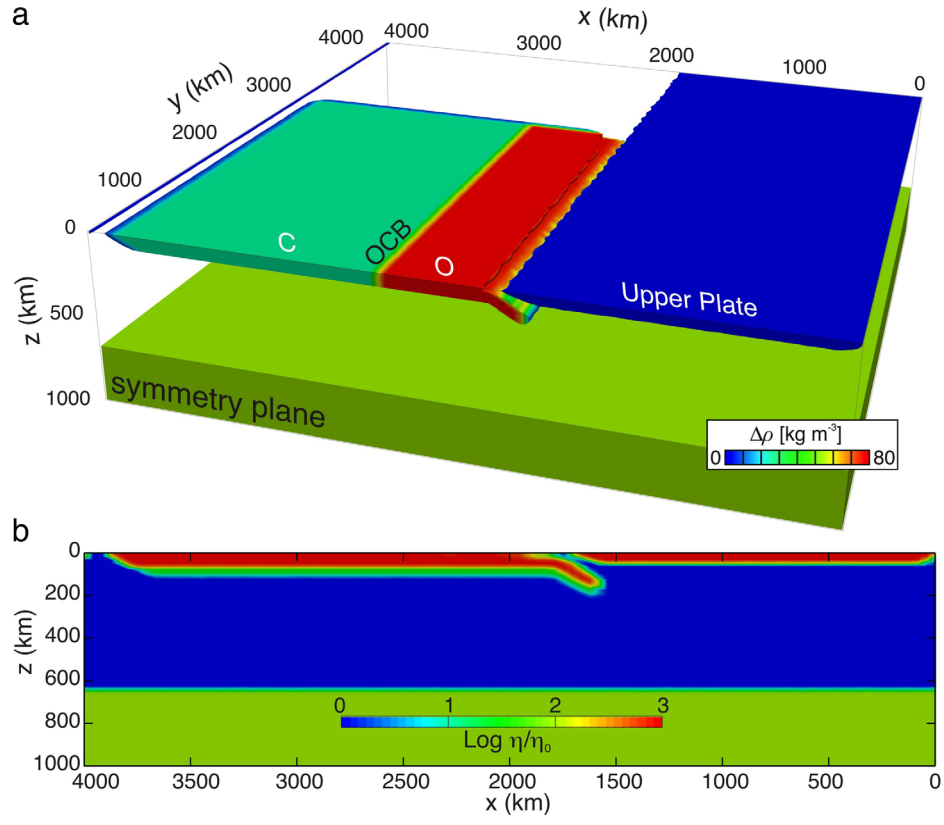

Figure 3. Numerical model setup. (a) Density field in color showing the different domains, plotted over the contour of the initial viscosity field ($\eta = 10^{19}$ Pa s). The model is 4000 km × 4000 × km. The symmetry plane xz is in $y = 0$. Model parameters are given in Tables 1 and 2. (b) Viscosity distribution in the initial stage, in the symmetry plane.

and Newtonian viscosity of $10^3\eta_M$, in the initial models setup. The upper plate is fixed in the far field, that is its 100 km tail has an imposed velocity $\boldsymbol{u} = 0$. We have run most of the models with an upper plate with no constraints and free to move horizontally, as well as models with no upper plate (Table 2), although the mechanisms investigated here are almost reference frame-independent. In additional sets of models, we have varied the viscosity to $10^2\eta_0$, which is the observed effective viscosity of the deforming Asian lithosphere [*England and Molnar*, 1997]. We have also used a composite visco-plastic rheology to address the role of upper plate deformation during convergence, although the results are very similar to the lower viscosity upper plate models.

3. Results

3.1. Slab Buoyancy and Slab Breakoff

[20] In the first stage of the model evolution, a slab extending to the base of the upper mantle develops, followed by the steady-state subduction stage, during which slab accumulates atop the upper-lower mantle transition zone. This evolution is very similar in the models of subduction of an oceanic plate as well as those where a continental plate follows subduction, and are in agreement with the evolution of other published models driven by slabs negative buoyancy [e.g., *Stegman et al.*, 2010].

[21] When the slab breakoff during subduction is modeled, the slab morphology around the breakoff varies as a function of the density of the downgoing plate in time. The first case is that of an intraoceanic breakoff where the buoyancy of the lithosphere around the breakoff does not change (Figure 4a). In this case the entrained lithosphere's negative buoyancy is sufficient to drive self-sustaining subduction, despite the breakoff. The limbs of the lithosphere around the detachment sink at almost the same rate, and do not separate largely while subducting. This breakoff perturbation is transient, and once the detached lithosphere has reached the transition zone, subduction returns

Table 2. List of Model Runs and Parameters Used (if Different From Table 1)

Exp.	$\Delta\rho_C$ (kg m^{-3})	w (km)	Oc. Cohesion	η_{UP} (Pa s)
1	26.6	–	–	–
2	26.6	–	–	$3\times10^3\eta_0$
3	26.6	500	C_0	$3\times10^2\eta_0$
4	26.6	500	C_0	$3\times10^3\eta_0$
5	26.6	500	C_0	$3\times10^3\eta_0+\tau_Y$[a]
6	26.6	1000	C_0	$3\times10^2\eta_0$
7	26.6	1000	C_0	$3\times10^3\eta_0$
8	26.6	1000	C_0	$3\times10^3\eta_0+\tau_Y$
9	26.6	2500	C_0	$3\times10^2\eta_0$
10	26.6	2500	C_0	$3\times10^3\eta_0$
11	26.6	1000	$2\times C_0$[b]	$3\times10^2\eta_0$
12	26.6	1000	$2\times C_0$	$3\times10^3\eta_0$
13	26.6	1000	$2\times C_0$	$3\times10^3\eta_0+\tau_Y$
14	26.6	2500	$2\times C_0$	$3\times10^2\eta_0$
15	26.6	2500	$2\times C_0$	$3\times10^3\eta_0$
16	26.6	2500	$2\times C_0$	$3\times10^3\eta_0+\tau_Y$
17	26.6	500	C_0	–
18	26.6	2500	C_0	–
19	53.3	–	–	$3\times10^2\eta_0$
20	53.3	500	C_0	$3\times10^2\eta_0$
21	53.3	500	C_0	$3\times10^3\eta_0$
22	53.3	1000	C_0	$3\times10^2\eta_0$
23	53.3	1000	C_0	$3\times10^3\eta_0$
24	53.3	2500	C_0	$3\times10^2\eta_0$
25	53.3	2500	C_0	$3\times10^3\eta_0$
26	53.3	1000	$2\times C_0$	$3\times10^2\eta_0$
27	53.3	1000	$2\times C_0$	$3\times10^3\eta_0$
28	80	–	–	$3\times10^2\eta_0$
29	80	500	C_0	$3\times10^2\eta_0$
30	80	500	C_0	$3\times10^3\eta_0$
31	80	1000	C_0	$3\times10^2\eta_0$
32	80	1000	C_0	$3\times10^3\eta_0$
33	80	1000	C_0	$3\times10^3\eta_0+\tau_Y$
34	80	2500	C_0	$3\times10^2\eta_0$
35	80	1000	$2\times C_0$	$3\times10^2\eta_0$
36	80	2500	$2\times C_0$	$3\times10^2\eta_0$

[a]Composite visco-plastic rheology.
[b]Triggered propagating breakoff.

to the state prior to the breakoff. The subduction evolution is almost insensitive of the lithospheric failure.

[22] Instead, when the breakoff occurs at the OCB, the deeper negatively buoyant oceanic-like lithosphere and the shallower less negatively buoyant continental-like one separate progressively, following their different buoyancy. While the more negatively buoyant deep oceanic slab rapidly sinks in the mantle under its own weight, the less negative buoyancy shallower continental edge of the OCB sinks at a smaller rate. When the buoyancy subducting plate is reduced to 53.3 kg m^{-3}, the entrained continental lithosphere has sufficient negative buoyancy to follow subduction, but at smaller rates respect to the neighboring lithosphere, still attached to the oceanic slab (Figure 4b). The deep detached oceanic slab sinks, while the continental slab above the breakoff remains at shallow depth. Slab deformation accommodates the different dips along the trench. When the buoyancy of the subducting plate is reduced to 26.6 kg m^{-3}, the integrated buoyancy of the continental plate above the slab breakoff is not enough to drive self-sustaining subduction and remains accommodated at shallow depths, underthrusting the overriding lithosphere. In the case with the lowest continental lithospheric buoyancy tested, the effect of breakoff on the morphology, with underthrusting and ongoing subduction, is permanent.

[23] In their intermediate stage, that is when ~400 km of lithosphere have been subducted since

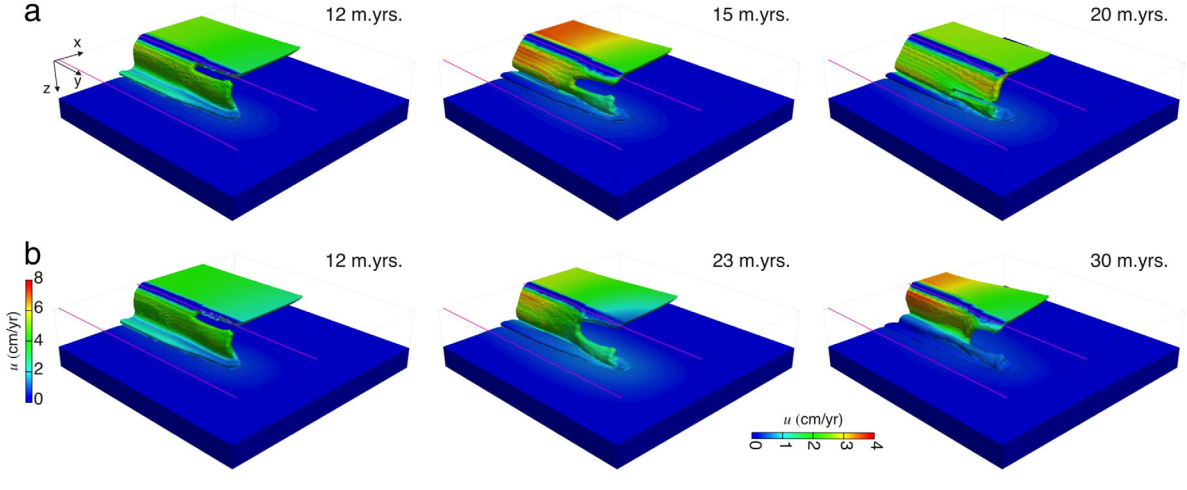

Figure 4. Time evolution of different models with partial breakoff: (a) intraoceanic breakoff, (b) break off at the OCB, continental density contrast of $\Delta\rho_C = 53.3$ kg m^{-3}. Contoured surface of the density field ($\Delta\rho = 60$ kg m^{-3}) with projection of the velocity magnitude. Note the different colorscales for the velocity in Figure 4b at 23 and 30 myr.

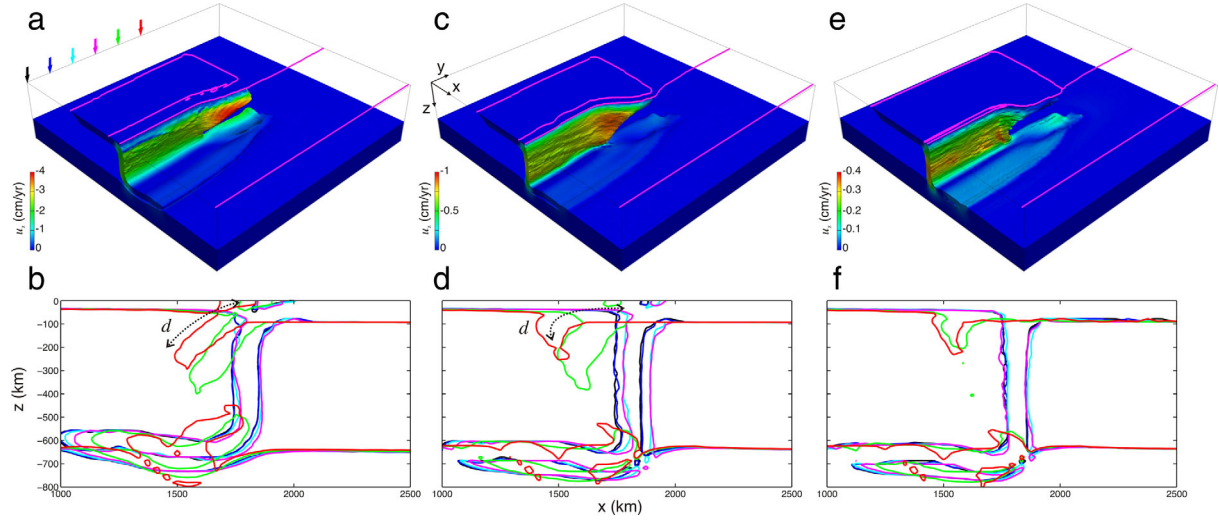

Figure 5. Subduction and breakoff models with a deformable upper plate. (a, c, and e) Contour of the density field with trace of the upper plate (in magenta) and vertical velocity in colorscale. (Figure 5a) Model with an intraoceanic detachment. (b) Color-coded cross sections of the viscosity field ($\eta = 10^{21}$ Pa s), taken at 500 km interval, locations are indicated by colored arrows on top of Figures 5a and 5c. Model with breakoff occurring at the OCB and $\Delta\rho_C = 53.3$ kg m^{-3}. (d) Cross sections of the model. (Figure 5e) Model with breakoff occurring at the OCB and $\Delta\rho_C = 26.6$ kg m^{-3}. (f) Cross sections of the model. The amount of underplating d is equal to the total lithosphere subducted since breakoff.

breakoff, the models attain similar morphology (Figure 5). The detached tip of the lithosphere has progressively overridden both the detached deeper slab and the position of the original trench, whereas laterally, the slab is continuous. In the different models the horizontal offset due to overriding is comparable. This depends on the total amount of subducted/underplating lithosphere d (Figure 5), and is equivalent to the amount of lithosphere entrained at the convergent margin since breakoff. Thus it is independent of the rates of subduction or slab buoyancy. The slab subduction has resumed in the intraoceanic detachment model (Figure 5a), instead in the continental models (Figures 5c and 5e) subduction did not resume, and the continental entrained plate is accommodated at shallow depths, underplating the upper plate.

3.2. Slab Breakoff Width

[24] We have tested instantaneous slab breakoff, either partial with total different width ($w = 500$, 1000km) or complete, as well as a breakoff that is triggered and then propagates laterally. The models' evolution is rather independent of the modality of breakoff and all the continental subducting slabs develop the same curved morphology.

[25] In Figure 5 we show different breakoff modalities at the stage when subduction has resumed and the OCB has almost reached the transition zone. In these models, all having continental densities of 26.6 kg m^{-3}, subduction has resumed after the breakoff in the centre of the slab, whereas at the margin's edge the lithosphere above the tear does not follow subduction, and remains accommodated at shallow depth (Figure 6).

[26] While the continental lithosphere above the tear remains at shallow depth, away from the initial breakoff the slab is steep (Figure 6). The effect of the propagation of the breakoff is to smooth the transition between steep and underplating slabs, respect to the partial breakoff. Surprisingly, the same morphology develops in the model where the breakoff had removed completely the slab at shallow depth (Figure 6c, inset). This is due to the effect of the mantle flow. The mantle flow around subducting slabs varies laterally along the trench from poloidal in the center to toroidal at the slab edge (Figure 7a). In the slab center the vertical convective cell extends throughout the upper mantle and couples the portions of slabs around the breakoff, until subduction becomes self-sustaining (Figure 7b). When the slab vertical continuity is lost due to the breakoff, stresses still propagate from the sinking slab to surface through the mantle viscous coupling. Consequently, the slab tip attains a relatively large vertical velocity. Instead, at the slab edge, the toroidal flow does not effectively drag the shallow lithospheric tip into the

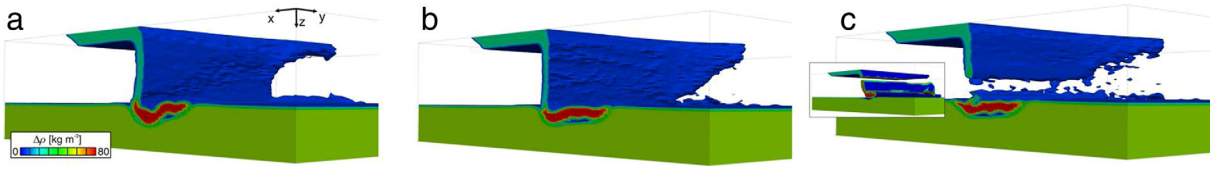

Figure 6. Models with (a) partial breakoff $w = 500$ km, (b) laterally propagating breakoff and (c) complete breakoff. Inset in Figure 6c, initial configuration of the complete slab breakoff. The models are shown when subduction has resumed and ~620 km of continent have subducted. Contoured surface of the density field.

mantle. The vertical convection cell here is reduced to the flow around the deep detached slab, which remains relatively less coupled to the surface, and the vertical velocity of the slab tip at the edge has completely vanished (Figure 7c). Above the slab breakoff, the downgoing plate is dragged to the convergent margin by lateral stress propagated through the plate, resulting in a strong coupling to and indentation of the upper plate. The progressive widening of the slab tear is followed by the migration of the toroidal component toward the centre of the slab, and the final morphology achieved is that of a gradually deepening slab tip, from the edge to the center. In models with larger negative buoyancy this effect is smaller, as the buoyancy of the lithosphere after breakoff sustains subduction.

3.3. Convergent Motions

[27] In the models presented here, the integrated buoyancy of the slabs drives the motions of subduction. We show the convergence velocity u_{conv} during the evolution of the subduction models (Figure 8), which is equal to the subducting plate velocity, as the upper plate is fixed.

[28] In all the models, the convergence velocity increases from the beginning of the simulation until the slab reaches the transition zone, ~7 myr (Figure 8a), and is followed by a decrease at ~11 myr when part of the slab is supported by the lower mantle. In the oceanic subduction models where no buoyancy change is imposed in the subducting plate, the convergence velocity follows the periodically piling of the slab at depth, with velocity variations between 4 and 7 cm yr^{-1} (Figure 8a, black line). In the subduction models with continent buoyancy drop to 53.3 kg m^{-3}, convergence rate decreases and reaches ~2 cm yr^{-1} within ~15 myr from the entrainment of the OCB (Figure 8a, red line). In the continental subduction models with a continental buoyancy of 26.6 kg m^{-3}, the subduction rate decreases reaching a steady-state velocity of ~1 cm yr^{-1} within ~30 myr (Figure 8a, green line). With the

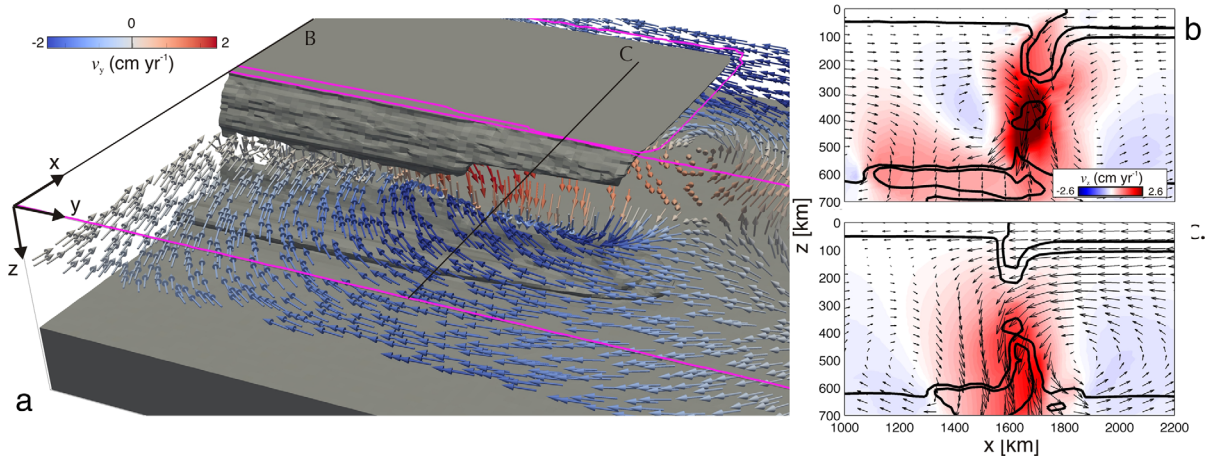

Figure 7. Mantle flow and velocity with complete breakoff model (Figure 4c). The model is shown when the slab has detached completely from the lithosphere at surface and deeper slab has reached ~330 km depth. (a) Mantle flow on the horizontal section taken at mid mantle depth ($z = 300$ km) and color scaled for u_y and contour of the viscosity field in gray. In magenta, the contour of the viscosity field on the surface ($\eta = 10^{21}$ Pa s), showing the upper plate, and location of the cross sections. (b) Cross section at the symmetry plane, with contour of the viscosity in black and mantle flow vectors in black. Color scale is for the (downward) vertical velocity u_z.

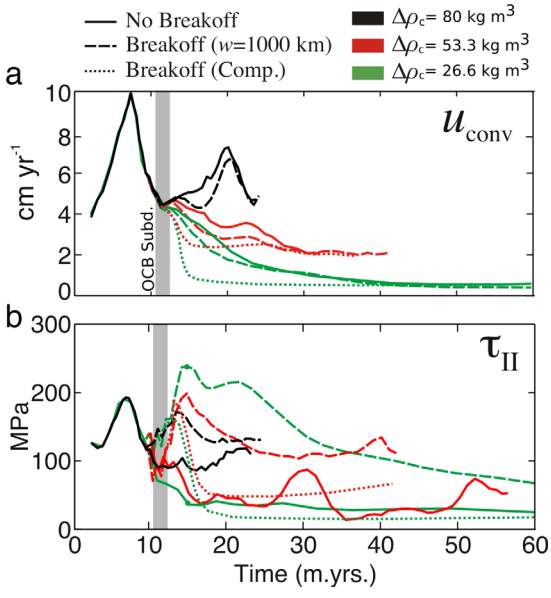

Figure 8. (a) Time evolution of convergence rate u_{conv} and (b) upper plate second invariant of the stress tensor τ_{II} in models of continuous subduction (solid lines), models of partial break off (dashed lines) and complete breakoff (dotted lines). The dots on the green lines in Figure 8b indicate the timestep in Figure 9. The gray vertical line indicates the time when the OCB is subducted.

entrainment of relatively lighter slabs, the driving force progressively reduces, and so does the convergence rates.

[29] Partial slab breakoff effect on the convergence rates is minor (Figure 8a, dashed lines) and the general trends observed before are reproduced. The impact of the partial (and propagating) slab breakoff is minor on the convergence because a large portion of the slab is still coherent and can support the weight of the slab, propagating stresses to the surface, pulling the rigid plate toward the trench [e.g., *Yoshioka and Wortel*, 1995].

[30] In the limit case of the complete breakoff, which removes almost instantaneously the slab pull, the convergence rate drops very rapidly (<5 myr) with all the continental buoyancies tested (Figure 8, dotted lines). However, convergence does not halt, and instead attains rapidly the asymptotic velocity. This is because the subduction resumes almost instantaneously after breakoff at the rate pertaining to the continental buoyancy.

3.4. Stress Transfer Across Convergent Margins

[31] The coupling between the upper plate and the subducting slabs occurs the flow in the viscous mantle in the wedge above the sinking slab. As a consequence, the stress in the upper plate scales with the buoyancy of the subducting slab as shown by previous modeling studies [*Capitanio et al.*, 2010b; *Capitanio et al.*, 2011].

[32] In all the models part of the stress is accommodated along a narrow belt near the convergent margin, therefore to estimate the intraplate stress far from margins we have measured the stress at a distance of ~200 km from the trench. The upper plate stress reaches a peak during the initial phase of subduction (Figure 8b), as the integrated buoyancy force of the slab increases with the

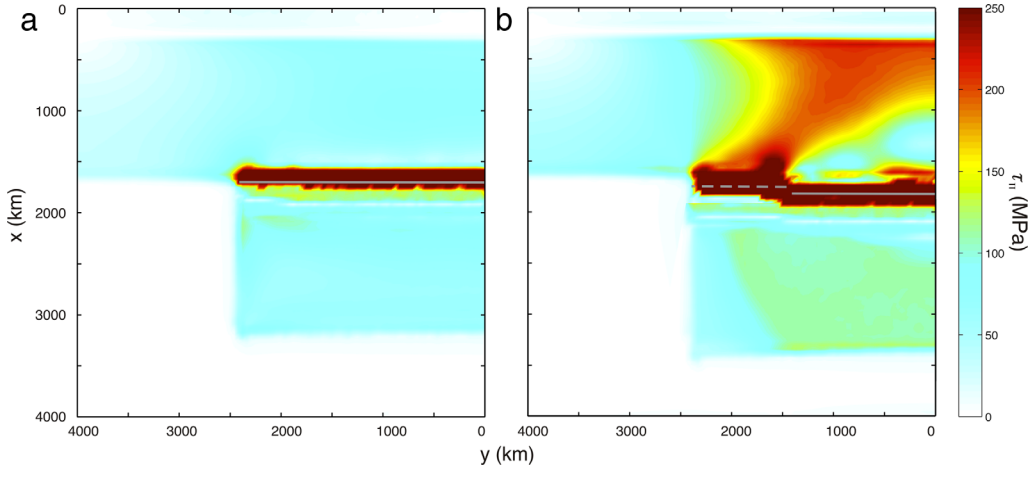

Figure 9. Top view of second invariant of the stress tensor τ_{II} in the models of (a) continuous subduction and (b) breakoff during subduction. The solid gray line indicates the trench that is continuous to the slab at depth, the dashed gray line indicates the projection of the broken off slab. The time steps are indicated in Figure 4 with green dots.

development of a slab from surface to the bottom of the upper mantle. In the models with a coherent slab, after this initial phase, the stress decreases to a rather constant low value (solid lines). Short period, minor stress variations are observed in the oceanic and high-buoyancy continental upper plate (Figure 8b, black and red solid lines), essentially due to slab piling atop the lower mantle that periodically put the upper plate in compression [i.e., *Capitanio et al*., 2010b]. Despite the piling is similar, this effect is not seen in the low-buoyancy continental upper plate (Figure 8b, green solid line), as the low rates of subduction allows for larger slab deformations accommodating the stresses within the slab, not at the surface.

[33] Instead, in models experiencing slab breakoff, a transient upper plate stress surge follows rapidly the OCB entrainment and the slab breakoff (Figure 8b, dashed lines). The upper plate stress peaks 2 to 4 myr after the breakoff. As less negatively buoyant continent is subducted, available pull forces progressively lower, and consequently upper plate stress decreases. The decay of the upper plate stress is longer the lower the subduction rates, reaching a relatively constant value after 4–5 myr for the oceanic plate subduction, 14 myr for the dense continent and up to ~20 myr for the lighter continent. Peak stresses in excess of ~240 MPa are achieved when the continental buoyancy is the minimum tested, and is 200 and ~170 MPa in maximum continental and oceanic buoyancies models, respectively. First, this shows that the coupling between lower and upper plates is inversely proportional to the buoyancy of the subducting plate above the breakoff. If the lower plate is less prone to subduction, it will couple more effectively to the upper plate when pulled toward the trench. Second, the progressive entrainment of relatively buoyant slab decreases the driving force, decreases convergence rates, and decreases stress available at the convergent margin, hence determining the transient nature of the stress surge.

[34] For the complete slab breakoff model, a rapid drop in the upper plate stresses follows the pull force removal (Figure 8b, dotted lines), with a duration similar to the convergence rate drop, ~5 myr The upper plate transitions almost instantaneously to low-stress regime. When breakoff propagates laterally, the evolution of the stresses is very similar to that of the partial breakoff models.

[35] One striking result is that the upper plate stresses are rather diffuse in the models with a coherent slab at depth, and is instead strongly localized in the upper plate when breakoff occurs (Figure 9). In the models with a coherent slab, shearing at the interplate margin accommodates the stress at surface (Figure 9a). No localization is observed within the upper plate, and the low stress measured is representative of an average over the whole upper plate. Instead, in the models where the breakoff occurs, the distribution of the stress in the upper plate is strongly localized, increasing largely above the tip of the slab breakoff at depth (Figure 9, gray dashed line for breakoff). In this case, all the models show the same pattern of a stress belt propagating largely into the upper plate for ~1200 km at an angle with the trench of 45° ± 5°. This is the result of stress coupling gradients at the trench, which to the first order reflect the distribution of slab mass at depth, and thus less dependent on the rheologies used (Figure 7c)

[36] The upper plate stress time evolutions explain that large stresses are triggered only at the incipient phase of the breakoff, and although the stress belt migrates with the lateral propagation of the slab tear, stresses become negligible soon. Thus, intracontinental deformations in the upper plates follow the incipient breakoff and rapidly vanish, irrespective of the lateral propagation of breakoff tears.

3.5. Convergent Margin Curvature

[37] The models with a lowered viscosity upper plate present the same subduction evolution of those presented earlier, however the interactions of the slab accommodated at shallow depth allow for plate and margin deformations (Figure 10).

[38] We found that all the models develop the same curvature and offset, whereas the width of detachment has a secondary control on the indenter morphology. In the models with a partial slab breakoff 500 km wide, the curvature increases with time (Figure 10a), and eventually the indenter becomes cusp-like. With a slab breakoff reaching a width of 1000 km, the curvature evolution is very similar, however the indenter has a wide and rather flat head (Figure 10b). The trench curvature and the length of the curved trench portion depend on the excess slab pull applied at the tear tip and on the stiffness of the deforming plate (i.e., the lithosphere-mantle viscosity contrast), this is the same in these models and thus the curvature does not change. Yet when the lateral width of the detachment is smaller than the characteristic length (~700 km), the indenter develops a cusp

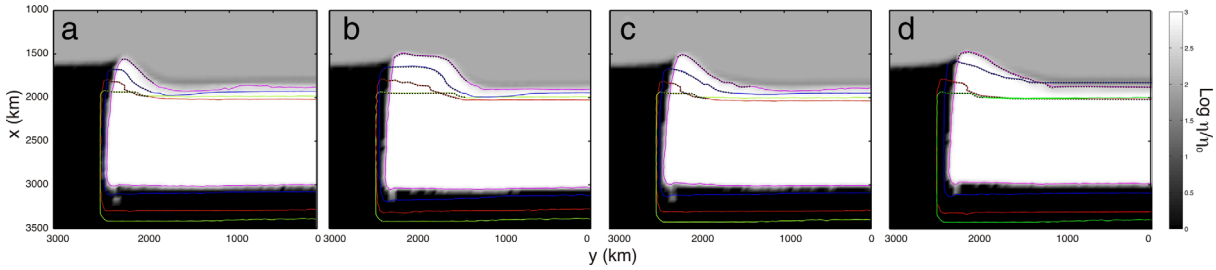

Figure 10. Evolution of the curvature of the trench with different slab breakoff mechanisms. Top view of the viscosity field at the final timestep (gray scale) with and contour at the surface, for $10^3\eta_0$ (magenta contour). Additional contours in colors at different stages, i.e., when the same amount of lithosphere has been consumed. The width of the slab tear at depth is projected to the margin (black dashed line). (a) Breakoff $w = 500$ km (b) Breakoff $w = 1000$ km. (c) Propagating breakoff. (d) Complete slab breakoff.

shape. Instead, when the detachment lateral tip is at a larger distance from the plate edge, as in the model of breakoff width of 1000 km, the far end of the indenter is not perturbed by the excess load at depth during subduction, and keeps its original shape during indentation.

[39] In the model with a migrating slab detachment (Figure 10c) the progressive lateral shift of the breakoff tip, where the excess slab load is applied, induces a migration of the curvature, resulting in a cusp-like slab edge. The same results in models with a complete detachment occurring at shallow depth (Figure 10d). Although the slab is completely detached, gradients in the coupling grow until the slab extends to the bottom of the upper mantle (Figure 6).

[40] In the models with larger negative buoyancies the perturbation due to breakoff is transient and the curvature of the margin, similar to what presented so far, is recovered once the slab has fully developed again.

[41] The horizontal trench offset in the models is the same, showing that the upper plate rheology does not affect this process. As presented earlier, the offset is proportional to the amount of convergence (Figure 5).

4. Discussion

[42] While the long-distance migration of the Indian plate is likely related to far-field forces, driving large displacement of the continent toward the north [*Becker and Faccenna*, 2011; *Cande and Stegman*, 2011; *Capitanio et al*., 2010a], the deformation of the Asian convergent margin can be described in the Indian plate reference frame. In fact, the effects of the breakoff presented in the previous sections depend on the distribution of slab mass beneath the margin and the propagation of stress to the subducting and upper plate, which are independent of the migration rate of the subducting plate.

4.1. Controls on Western Syntaxis Formation

[43] During India-Asia convergence, a breakoff separated the subducting Tethys from the shallow Indian continental slab ~44–48 Ma [*Negredo et al*., 2007]. It has been inferred that the slab breakoff occurred roughly at the same time all along the northern margin of continental India as the tomographic anomaly attenuates and vanishes roughly at the same depth along the trench (Figure 1). The breakoff time marks the change from the linear Asian margin during Tethys subduction to the progressive curvature of the trench, suture and Himalayan front during to the northward migration of the Indian continent [*Replumaz et al*., 2004].

[44] Our models show that the margin curvature and underplating develops as a consequence of the breakoff. Similar geometry to the models is found beneath the Pamir, where Indian lithosphere underplates the Asian plate overriding its shallow detached slab portion, whereas to the east, the slab is rather vertically continuous. The present day morphology (Figure 1) shows that ~650 km of Indian lithosphere has been accommodated beneath the Asian plate in the Western Syntaxis, since the breakoff, which has only recently (~8 Ma) started to subduct [*Negredo et al*., 2007]. This morphology is compatible with the models and is rather independent of the modality of breakoff.

[45] In our models the trench curvature is proportional to the subducting plate stiffness, once the upper plate is weakened, and is very similar to the

curvature of the Indian plate margin, where the upper plate viscosities are comparable to those used here [*England and Molnar*, 1997]. On the other hand, the location of the curvature on the western end of the Indian margin might be the result of two mechanisms related to breakoff: the nucleation of the partial/propagating breakoff at the slab border, or the mantle flow constraints in the case of a total breakoff. In the Indian case of complete slab breakoff, the margin's western end was rapidly separating from the Tethys slab, vertically as well as horizontally, due to the Indian northward migration, as suggested by the tomography [*Negredo et al*., 2007], and thus likely allowed for toroidal flow. Instead, to the center, the toroidal flow would locally vanish and the poloidal flow maximized, instead. The implication of this configuration is that subduction would have resumed in the central Indian trench after the separation of the Tethys from Indian slab, and instead hampered along the western end, irrespective of in the breakoff dynamics. The models curvature following the breakoff develops inside the trench, whereas the deformation in the upper plate outside of the margins, i.e., laterally, is almost negligible.

4.2. Controls on Asian Indentation Tectonics

[46] Our results show that the loss of slab mass along the margin during subduction controls the coupling and the stress transfer across the margin. We found that along-trench gradients in the coupling are in the first order controlled by the slab mass and its distribution at depth, altered by the local loss of mass that follow the breakoff, which are independent of the choice of mantle rheology. Along-trench coupling gradients lead to stress localization on the upper plate and the propagation along a belt at an angle with the trench of ~45°. This latter departs from the projection of the slab tear tip on the trench, where slab pull gradient is steepest. In the models the stress surge is transient, it shortly follows the breakoff and vanishes within <5 to 10 s of myr The similar trends of the strike-slip faults and the stress belt in the models support the interpretation of the formation of widespread strike-slip faulting during collision, as illustrated in the tectonics reconstructions (Figure 1) [*Replumaz and Tapponnier*, 2003; *van Hinsbergen et al*., 2011a; *Yin*, 2010], as a consequence of the breakoff episodes.

[47] We suggest that the symmetric faults forming a frontal triangle represented in the tectonics reconstructions at the onset of indentation around 45–40 Ma, could be related to the breakoff occurring at the OCB at 45 Ma [*Negredo et al*., 2007], with breakoff propagation from both east and west extremities of the Indian continent. Such morphology has been inferred from the tectonic reconstructions and analogue experiments, where the bounding faults isolate a triangular block in front of the indenter, the western part of the triangle following the Bangong suture [*Replumaz and Tapponnier*, 2003; *Peltzer and Tapponnier*, 1988]. The trend of the Bangong suture at its initiation was at ~45° from the plate margin (Figure 2), compatible with the models' stress belt in the upper plate generated by the slab breakoff. The reconstructed intersection with the trench was close to the western corner of the Indian continent [*Replumaz and Tapponnier*, 2003] east of the present-day Western Syntaxis, which is compatible with the models. We thus propose that the older breakoff provided transient large stresses that passed the strength of the Asian lithosphere reactivating the Bangong suture (Figure 2). This tectonic rearrangement is coeval to the tearing of the Indian slab between the western (HK) and the central (IN) Indian margin, occurring between 40 and 30 Ma [*Replumaz et al*., 2010b]. Between 30 and 15 Ma, the Indochina block extruded eastward along the Bangong-RRF (Figure 2) [*Replumaz and Tapponnier*, 2003; *Leloup et al*., 2001], following the propagation of the Bangong suture eastward connecting with the RRF.

[48] Following the extrusion, the deformation migrated to the north of the Asian continent, and new major faulting initiated in this time: the Chaman, the Karakorum, the Kunlun and the ATFs (Figure 2) [*Replumaz and Tapponnier*, 2003; *van Hinsbergen et al*., 2011a; *Yin*, 2010]. The trend and the trench intersection point of the models' upper plate stress belt are comparable to those of the Chaman fault and the ATF close to the western end of the margin (Figure 2) [*Tapponnier and Molnar*, 1976]. The ATF is the younger strike-slip fault activated during the collision, along which thickening migrates to the north of the Tibetan Plateau, at least since 15 Ma [*Replumaz and Tapponnier*, 2003]. The Chaman could have been activated at about 25 Ma, coeval with the Pamir subduction [*Burtman and Molnar*, 1993]. It is timely related to the Indian slab breakoff episode occurring within the continental slab (IN) and propagated from the westernmost border of the remaining slab toward the east, over a time span of ~10 myr between 25 and 15 Ma [*Replumaz et al*., 2010b]. We propose that this younger breakoff

provided the stresses necessary to renew faulting to form the ATF, and contemporaneous faults east and north in the Asian continent.

4.3. Controls on Convergent Motions

[49] According the buoyancy principle our models illustrate, the entrainment of a lithosphere with very low negative buoyancy explains the long-lived Indian underplating beneath the Western Syntaxis. The underplating in the Western Syntaxis lasted since the break off age until ~8 Ma, when the Indian lithosphere then subducts to large depth [*Koulakov and Sobolev*, 2006; *Negredo et al*., 2007]. Such long-lived feature requires the continuous entrainment of a very low negative buoyancy lithosphere, i.e., a continent, since breakoff. Our models show that a maximum plate negative (equivalent) buoyancy of ~26–20 kg m^{-3} for a 80–100 km thick lithosphere is required to achieve the long-lived underplating imaged beneath the Western Syntaxis. These values are likely those of a continental lithosphere undergone some degree of metamorphism/eclogitization [*Cloos*, 1993], and represent the upper limit of the continental buoyancies.

[50] The entrainment of such lower buoyancy plate affects the subduction motions, and should thus also impact the India-Asia convergence rates [*Patriat and Achache*, 1984]. The subduction of continental-type buoyancy lithosphere results in a relative reduction of convergence rates of ~3 times in 10–20 myr, and is comparable to the India-Asia convergence reduction of a similar factor achieved between ~50–55 and ~35–40 Ma. In fact, the causes of the Meso-Cenozoic Indian plate motions are still debated. Various hypotheses have been proposed including the increase of resisting forces, either due to the topography [*Copley et al*., 2010] or upper plate resistance [*Clark*, 2012], the contribution of external forces, as the transient effect of a plume [*Cande and Stegman*, 2011; *van Hinsbergen et al*., 2011b], or the decrease of the driving force, due to continent subduction [*Capitanio et al*., 2010a], as in here. Although it is likely that these different forces might be at work, the slab pull force is the most fundamental driver of plate motions [*Forsyth and Uyeda*, 1975], so that the decrease of driving force that follows the Indian continent subduction and breakoff should play a first-order control on the convergence rate drop [*Capitanio et al*., 2010a].

[51] The velocity drop in the India-Asia convergence is compatible with the models' evolution where driving forces changed gradually, with progressive entrainment of continental lithosphere. Reviewed reconstructions of the India-Asia kinematics report more abrupt velocity drops in this period [*van Hinsbergen et al*., 2011b; *White and Lister*, 2012], which is expected to result from complete breakoff during subduction, although this interpretation remains speculative. More in general, a noncoeval impingement of low-buoyancy lithosphere in the trench is more compatible with the reconstructions of the Greater Indian margin [*Ali and Aitchinson*, 2005; *Gibbons et al*., 2012; *Zahirovic et al*., 2012], and geological evidence from the western Himalayan horizontal polarization terrains [*Guillot et al*., 2007]. Yet we have shown that the convergence of such a large plate responds to the slab buoyancy averaged over the trench and is thus possible that the lithosphere subducted included some portions of oceanic lithosphere still open to the east. This would then delay the "collision" recorded in the Himalayan orogen [*Aitchinson et al*., 2007].

[52] It is important to note that partial and propagating slab breakoff, and to a certain extent also the complete, instantaneous slab detachments, induce minor convergent motions variations, O(1–2 cm yr^{-1}). This shows that the coupling gradients formed at the trench due to breakoff might have a minor role in the plate kinematics, unable to reliably constrain such minor variations, yet alter significantly the boundary forces propagating from margin into the deforming upper plates.

4.4. Different Deformation Styles Along the Indian Convergent Margin

[53] The new insights discussed offer the key to interpret the formation and occurrence of different deformation styles in Central Asia as the consequence of continental subduction and slab breakoff. During convergence, far-field forces can increase the coupling with the upper plate, resulting in trench migrations onto the Asian upper plate [*Capitanio et al*., 2010a; *Chemenda et al*., 2000]. Although this reconciles the model originally proposed for the indentation tectonics [*Tapponnier and Molnar*, 1976] with subduction dynamics, this mechanism is not compatible with other deformation styles, coeval to the major faulting, as the underplating in the Western Syntaxis and the thickening of the Tibetan plateau [*Royden et al*., 2008]. Mechanics arguments suggest that the plastic [*Tapponnier et al*., 1982] and the viscous deformation [*England and McKenzie*, 1982] in front of

a migrating margin could not coexist: whether deformation is accommodated by viscous thickening [*England and McKenzie*, 1982] or faulting and thrusting [*Tapponnier and Molnar*, 1976; *Tapponnier et al*., 2001] these both require that the stress remained constantly below or above the yield limit of a (elasto-)viscoplastic lithosphere, respectively. The continuous thickening of the Tibetan plateau requires constant rate of strain in the upper plate since collision, imposed by the convergence velocity boundary conditions [*Clark*, 2012]. But, constant strain rates are incompatible with different styles, as the viscous and the plastic major faulting, since these require substantially different stresses/strain rates, below and above the lithospheric strength, respectively.

[54] Instead, we have shown that breakoff episodes provide additional short-lived and localized large stresses at the margin that change the boundary conditions to the upper plate, whereas they do not alter the dynamics of subduction that drives convergent motions. Therefore, surge in the stress transfer across the Indian convergent margin, possibly above the Asian lithosphere yield limit, could have added to that imposed by convergence, forcing episodic faulting.

[55] According to our models, the stress surge is very localized, and is compatible with much lower stresses elsewhere in the upper plate, where the deformation remains controlled by the large-scale subduction, as shown by the coexistence of the Tibetan thickening with the Bangong-RRF and ATF faulting. Such fault discontinuities remain as permanent lithospheric weaknesses, so that they can accommodate continuously strain in time, although at lowered rates, also when the stress pulse vanishes, shortly after breakoff. In this way, plastic deformation on the major Asian faults could have been accommodate at the same time of the thickening in Tibet and the underplating in the Western Himalayan Syntaxis, explaining the long-lived coexistence of three different deformation mechanisms in Central Asia.

5. Conclusions

[56] We use three-dimensional numerical models of subducting-overriding lithospheres and mantle to test the role of continental subduction and slab breakoff during convergence. The force balance perturbations introduced by the slab breakoff have a minor impact on the convergence velocities, showing that this process does not affect the dynamics driving convergent motions. Yet breakoff episodes have a large impact on the coupling stresses with the upper plate and the deformation of this latter. The models' trench progressive curvature is the consequence of the breakoff, with ongoing underplating at the free edge of the slab and continuous subduction away from slab edge. The present-day morphology of the Indian slab suggests that similar processes occurred during the India-Asia convergence and the development of the underplating in the Western Syntaxis laterally continuous to subduction beneath Tibet, showing that this convergence zone was fundamentally controlled by breakoff episodes. Transient large-stress surge in the upper plates follows breakoff, forming a localized stress belt propagating away from the convergent margin. The location, strike and timing of the stress surge in the models match that of the major lithospheric faulting of the Bangong-RRF and ATF and the inferred breakoff episodes, showing that this is a viable mechanism to explain the inception of the indentation tectonics. Lithospheric discontinuities formed during episodes of large coupling remain as permanent features, as well as the long-lived underplating, also found along the margin. Consequently, Asian faulting and Western Himalayan Syntaxis underplating accommodated ongoing deformation at the same time of the convergence-driven Tibetan growth, explaining the coexistence of different deformation mechanisms in the Central Asian tectonics.

Acknowledgments

[57] This research was supported by the Australian Research Council Discovery Projects DP0987374 and DP110101697 and DECRA DE130100604 awarded to F.A.C. We thank T. Gerya and an anonymous reviewer for the comments on the manuscript.

References

Aitchinson, J. C., J. R. Ali and A. M. Davies (2007), When and where did India and Asia collide?, *J. Geophys. Res.*, *112*, BO5423, doi:10.1029/2006JB004706.

Ali, J. R., and J. C. Aitchinson (2005), Greater India, *Earth Sci. Rev.*, *72*, 169–188.

Becker, T. W., and C. Faccenna (2011), Mantle conveyor beneath the Tethyan collisional belt, *Earth Planet. Sci. Lett.*, *310*, 453–461.

Briais, A., P. Patriat and P. Tapponnier (1993), Updated interpretation of magnetic-anomalies and sea-floor spreading stages in the South China Sea—Implications for the Tertiary tectonics of South-Asia, *J. Geophys. Res.*, *98*(B4), 6299–6328.

Buiter, S. J. H., R. Govers and M.J.R. Wortel (2002), Two-dimensional simulations of surface deformation caused by slab detachment, *Tectonophysics*, *354*(3–4), 195–210.

Burkett, E. R., and M. I. Billen (2010), Three-dimensionality of slab detachment due to ridge–trench collision: Laterally simultaneous boudinage versus tear propagation, *Geochem. Geophys. Geosyst.*, *11*, Q11012, doi:10.1029/2010GC003286.

Burtman, V. S., and P. Molnar (1993), *Geological and Geophysical Evidence for Deep Subduction of Continental Crust Beneath the Pamir*, pp. 76, Geol. Soc. Am.

Cande, S. C., and D. R. Stegman (2011), Indian and African plate motions driven by the push force of the Réunion plume head, *Nature*, *475*, 47–52.

Capitanio, F. A., G. Morra, S. Goes, R.F. Weinberg and L. Moresi (2010a), India-Asia convergence driven by the subduction of the Greater Indian continent, *Nat. Geosci.*, *3*(2), 136–139.

Capitanio, F. A., D.R. Stegman, L. Moresi and W. Sharples (2010b), Upper plate controls on deep subduction, trench migrations and deformations at convergent margins, *Tectonophysics*, *483*, 80–92.

Capitanio, F. A., C. Faccenna, S. Zlotnik and D.R. Stegman (2011), Subduction dynamics and the origin of Andean orogeny and Bolivian orocline, *Nature*, *480*, 83–86.

Chemenda, A. I., J.P. Burg and M. Mattauer (2000), Evolutionary model of the Himalaya-Tibet system: geopoem based on new modelling, geological and geophysical data, *Earth Planet. Sci. Lett.*, *174*, 397–409.

Clark, M. K. (2012), Continental collision slowing due to viscous mantle lithosphere rather than topography, *Nature*, *483*, 74–77.

Cloos, M. (1993), Lithospheric buoyancy and collisional orogenesis: Subduction of oceanic plateaus, continental margins, island arcs, spreading ridges, and seamounts, *Geol. Soc. Am. Bull.*, *105*, 715–737.

Copley, A., J.P. Avouac and J.-Y. Royer (2010), India-Asia collision and the Cenozoic slowdown of the Indian plate: Implications for the forces driving plate motions, *J. Geophys. Res.*, *115*, B03410, doi:10.1029/2009JB006634.

Davies, J. H., and F. von Blanckenburg (1995), Slab breakoff: A model of lithosphere detachment and its test in the magmatism and deformation of collisional orogens, *Earth Planet. Sci. Lett.*, *129*, 85–102.

Duretz, T., S.M. Schmalholz and T.V. Gerya (2012), Dynamics of slab detachment, *Geochem. Geophys. Geosyst.*, *13*, Q03020, doi:10.1029/2011GC004024.

England, P., and D. McKenzie (1982), A thin viscous sheet model for continental deformation, *Geophys. J. R. Astron. Soc.*, *70*, 295–321.

England, P., and G. A. Houseman (1985), Role of lithospheric strength heterogeneities in the tectonics of Tibet and neighbouring regions, *Nature*, *315*, 297–301.

England, P., and P. Molnar (1997), Active deformation of Asia: From kinematics to dynamics, *Science*, *278*(5338), 647–650.

Forsyth, D., and S. Uyeda (1975), On the relative importance of driving forces of plate motion, *Geophys. J. R. Astron. Soc.*, *43*, 163–200.

Gerya, T. (2011), Future directions in subduction modeling, *J. Geodyn.*, *52*, 344–378.

Gerya, T. V., D. A. Yuen and W. V. Maresch (2004), Thermomechanical modeling of slab detachment, *Earth Planet. Sci. Lett.*, *226*, 101–116.

Gibbons, A., U. Barckhausen, P. van den Bogaard, K. Hoernle, R. Werner, J. M. Whittaker and R. D. Müller (2012), Constraining the Jurassic extent of Greater India: Tectonic evolution of the West Australian margin, *Geochem. Geophys. Geosyst.*, *13*, Q05W13, doi:10.1029/2011GC003919.

Guillot, S., A. Replumaz, K. H. Hattori and P. Strzerzynski (2007), Initial geometry of western Himalaya and ultrahigh-pressure metamorphic evolution, *J. Asian Earth Sci.*, *30*, 557–564.

Hafkenscheid, E., M. J. R. Wortel and W. Spakman (2006), Subduction history of the Tethyan region derived from seismic tomography and tectonic reconstructions, *J. Geophys. Res.*, *111*, BO8401, doi:10.1029/2005JB003791.

Kind, R., and X. Yuan (2010), Seismic images of the biggest crash on earth, *Science*, *329*, 1479–1480.

Kosarev, G., R. Kind, S. V. Sobolev, X. Yuan, W. Hanka and S. Oreshin (1999), Seismic evidence for a detached Indian lithosperic mantle beneath Tibet, *Science*, *283*(5406), 1306–1309.

Koulakov, I., and S. V. Sobolev, (2006), A tomographic image of Indian lithosphere break-off beneath the Pamir-Hindukush region, *Geophys. J. Int.*, *164*, 425–440.

Kumar, P., X. Yuan, R. Kind and J. Ni (2006), Imaging the colliding Indian and Asian lithospheric plates beneath Tibet, *J. Geophys. Res.*, *111*, B06308, doi:10.1029/2005JB003930.

Leloup, P. H., et al. (2001), New constraints on the structure, thermochronology, and timing of the Ailao Shan-Red River shear zone, SE Asia, *J. Geophys. Res.*, *106*(B4), 6683–6732.

Leloup, P. H., E. Boutonnet, W. J. Davis and K. Hattori (2011), Long-lasting intracontinental strike-slip faulting: New evidence from the Karakorum shear zone in the Himalayas, *Terra Nova*, *23*, 92–99.

Levin, V., N. M. Shapiro, J. Park and M. H. Ritzwoller (2005), Slab portal beneath the western Aleutians, *Geology*, *33*(4), 253–256.

Li, C., R. D. van der Hilst, A. S. Meltzer and E. R. Engdahl (2008), Subduction of the Indian lithosphere beneath the Tibetan Plateau and Burma, *Earth Planet. Sci. Lett.*, *274*, 157–168.

Liu, L., and D. R. Stegman (2011), Segmentation of the Farallon slab, *Earth. Planet. Sci. Lett.*, *311*, 1–10.

Liu, L., and D. R. Stegman (2012), Origin of Columbia River flood basalt controlled by propagating rupture of the Farallon slab, *Nature*, *482*, 386–389.

Mattauer, M. (1986), Intracontinental subduction, crust-mantle décollement and crustal-stacking wedge in the Himalayas and other collision belts, *Geol. Soc. London Spec. Publ.*, *19*, 37–50.

Mattauer, M., P. Matte and J. L. Olivet (1999), A 3D model of the India-Asia collision at plate scale, *C. R. Acad. Sci.*, *328*(8), 499–508.

Mechie, J., et al. (2012), Crustal and uppermost mantle velocity structure along a profile across the Pamir and southern Tien Shan as derived from project TIPAGE wide-angle seismic data, *Geophys. J. Int.*, *188*, 385–407.

Meyer, B., P. Tapponier, L. Bourjot, F. Métivier, Y. Gaudemer, G. Peltzer, G. Shunmin and C. Zhitai (1998), Crustal thickening in Gansu-Qinghai, lithospheric mantle subduction, and oblique, strike slip controlled growth of the Tibet Plateau, *Geophys. J. Int.*, *135*, 1–47.

Molnar, P., and J. M. Stock (2009), Slowing of India's convergence with Eurasia since 20 Ma and its implications for Tibetan mantle dynamics, *Tectonics*, *28*, TC3001, doi:10.1029/2008TC002271.

Molnar, P., and P. Tapponnier (1975), Cenozoic tectonics of Asia—Effects of a continental collision, *Science*, *189*(4201), 419–426.

Moresi, L., F. Dufour and H. B. Mülhaus (2003), A lagrangian integration point finite element method for large deformation

modeling of viscoelastic geomaterials, *J. Comput. Phys.*, *184*, 476–497.
Morra, G., K. Regenauer-Lieb and D. Giardini (2006), On the curvature of oceanic arcs, *Geology*, *34*(10), 877–880.
Murphy, M. A., A. Yin, T. M. Harrison, S. B. Dürr, Z. Chen, F. J. Ryerson, W. S. F. Kidd, X. Wang and X. Zhou (1997), Did the Indo-Asian collision alone create the Tibetan plateau?, *Geology*, *25*(8), 719–722.
Nábelek, J., et al. (2009), Underplating in the Himalaya-Tibet collision zone revealed by the Hi-CLIMB experiment, *Science*, *325*, 1371–1374.
Negredo, A. M., A. Replumaz, A. Villaseñor and S. Guillot (2007), Modeling the evolution of continental subduction processes in the Pamir-Hindu Kush region, *Earth Planet. Sci. Lett.*, *259*, 212–225.
Patriat, P., and J. Achache (1984), India-Eurasia collision chronology has implications for crustal shortening and driving mechanism of plates, *Nature*, *311*, 615–621.
Peltzer, G., and P. Tapponnier (1988), Formation and evolution of strike-slip faults, rifts, and basins during the India-Asia collision: An experimental approach, *J. Geophys. Res.*, *93*(B12), 15,085–15,117.
Regard, V., C. Faccenna, J. Martinod and O. Bellier (2005), Slab pull and indentation tectonics: Insights from 3D laboratory experiments, *Phys. Earth Planet. Inter.*, *149*, 99–113.
Replumaz, A., and P. Tapponnier (2003), Reconstruction of the deformed collision zone between India and Asia by backward motion of lithospheric blocks, *J. Geophys. Res.*, *108*(B6), 2285, doi:10.1029/2001JB000661.
Replumaz, A., H. Kárason, R. D. van der Hilst, J. Besse and P. Tapponnier (2004), 4-D evolution of SE Asia's mantle from geological reconstructions and seismic tomography, *Earth Planet. Sci. Lett.*, *221*, 103–115.
Replumaz, A., A. M. Negredo, S. Guillot and A. Villaseñor (2010a), Multiple episodes of continental subduction during India/Asia convergence: Insight from seismic tomography and tectonic reconstruction, *Tectonophysics*, *483*, 125–134.
Replumaz, A., A. M. Negredo, A. Villaseñor and S. Guillot (2010b), Indian continental subduction and slab break-off during Tertiary collision, *Terra Nova*, *22*, 290–296.
Replumaz, A., et al. (2012), Amount of Asian lithospheric mantle subducted during the India/Asia collision, *Gondwana Res.*, doi:10.1016/j.gr.2012.07.019, in press.
Royden, L. H., B. C. Burchfiel and R. D. van der Hilst (2008), The geological evolution of the Tibetan plateau, *Science*, *321*, 1054–1058.
Stegman, D. R., J. Freeman, W. P. Schellart, L. Moresi and D. May (2006), Influence of trench width on subduction hinge retreat rates in 3-D models of slab rollback, *Geochem. Geophys. Geosyst.*, *7*, Q03012, doi:10.1029/2005GC001056.
Stegman, D. R., R. Farrington, F. A. Capitanio and W. P. Schellart (2010), A Regime diagram for subduction styles from 3-D numerical models of free subduction, *Tectonophysics*, *483*, 29–45, doi:10.1016/j.tecto.2009.1008.1041.
Tapponnier, P., and P. Molnar (1976), Slip-line field theory and large-scale continental tectonics, *Nature*, *264*, 319–324.
Tapponnier, P., G. Peltzer, A.Y. Le Dain, R. Armijo and P. Cobbold (1982), Propagating extrusion tectonics in Asia: New insights from simple experiments with plasticine, *Geology*, *10*, 611–616.
Tapponnier, P., X. Zhiqin, F. Roger, B. Meyer, N. Arnaud, G. Wittlinger, and Y. Jinsui (2001), Oblique stepwise rise and growth of the Tibet plateau, *Science*, *294*, 1671–1677.
Van der Voo, R., W. Spakman and H. Bijwaard (1999), Tethyan subducted slabs under India, *Earth Planet. Sci. Lett.*, *171*, 7–20.
van Hinsbergen, D. J. J., P. Kapp, G. Dupont-Nivet, P. C. Lippert, P. G. DeCelles and T. H. Torsvik (2011a), Restoration of Cenozoic deformation in Asia and the size of Greater India, *Tectonics*, *30*, TC5003, doi:10.1029/2011TC002908.
van Hinsbergen, D. J. J., B. Steinberger, P. V. Doubrovine and R. Gassmöller (2011b), Acceleration and deceleration of India-Asia convergence since the Cretaceous: Roles of mantle plumes and continental collision, *J. Geophys. Res.*, *116*, B06101, doi:10.1029/2010JB008051.
van Hunen, J., and M. B. Allen (2011), Continental collision and slab break-off: A comparison of 3D numerical models with observations, *Earth Planet. Sci. Lett.*, *302*, 27–37.
White, L. T., and G. S. Lister (2012), The collision of India with Asia, *J. Geodyn.*, *56-57*, 7–17.
Wong A. Ton, S. Y. M., and M. J. R. Wortel (1997), Slab detachment in continental collision zones: An analysis of controlling parameters, *Geophys. Res. Lett.*, *24*(16), 2095–2098.
Wortel, M. J. R., and W. Spakman (2000), Subduction and slab detachment in the Mediterranean-Carpathian region, *Science*, *290*, 1910–1917.
Yin, A. (2010), Cenozoic tectonic evolution of Asia: A preliminary synthesis, *Tectonophysics*, *488*(1-4), 293–325.
Yoshioka, S., and M. J. R. Wortel (1995), Three-dimensional numerical modeling of detachment of subducted lithosphere, *J. Geophys. Res.*, *100*(B10), 20,223–20,244.
Yuan, X., J. Ni, R. Kind, J. Mechie and E. Sandvol (1997), Lithospheric and upper mantle structure of southern Tibet from a seismological passive source experiment, *J. Geophys. Res.*, *102*(B12), 27,491–27,500.
Zahirovic, S., R. D. Müller, M. Seton, N. Flament, M. Gurnis and J. Whittaker (2012), Insights on the kinematics of the India-Eurasia collision from global geodynamic models, *Geochem. Geophys. Geosyst.*, *13*, Q04W11, doi:10.1029/2011GC003883.